Aerodynamic Model Development and Fidelity Assessment for eVTOL Predicted Handling Qualities

Agata Rylko
PhD Candidate
Politecnico di Milano
Milan, Italy

Marco Lovera
Full Professor
Politecnico di Milano
Milan, Italy

Giuseppe Quaranta
Full Professor
Politecnico di Milano
Milan, Italy

ABSTRACT

This paper presents preliminary results from the development of a Flight Simulation Model of a small-scale lift+cruise eVTOL, aimed at assessing Predicted Handling Qualities at low speeds. The study focuses on aerodynamic model development using a mid-fidelity solver. It investigates key phenomena, notably propeller interference and induction on aircraft components, with significant findings on the horizontal stabilizer. Several modelling challenges are discussed related to the computation of stability derivatives. The static stability derivatives calculation methodology was confirmed, while dynamic stability derivatives revealed an unexpected frequency dependency that needs to be revised. The model will be used in the future to assess the uncertainty of the derivatives and investigate their impact on simulations. This work lays the foundations for further model development and fidelity assessment, contributing to credibility and supporting the demonstration of compliance with the handling quality requirements included in the Special Condition VTOL through simulation.

NOTATION

Acronyms

CFD Computational Fluid Dynamics

EASA European Union Aviation Safety Agency

eVTOL electric Vertical Take-off and Landing

FSM Flight Simulation Model

FTM Flight Test Maneuver

HQ Handling Qualities

MHQRM Modified Handling Qualities Rating Method

MTE Mission Task Element

RoCS Rotorcraft Certification by Simulation

VLM Vortex Lattice Method

VPM Vortex Particle Method

INTRODUCTION

In the Urban Air Mobility race, aiming for the first successful passenger-carrying commercial service using eVTOL aircraft, many brilliant engineers are currently paving the way towards the first eVTOL Type Certificate in Europe. The challenge is enormous, not only because of novelties introduced in the aircraft configurations, such as the distributed electrical propulsion and the employment of highly augmented flight control systems, but also leveled-up by very ambitious time schedules. In this undertaking, the eVTOL manufacturing companies are unveiling new technical challenges in aeronautical engineering, walking hand-by-hand with the regulators and guidelines developing organisations.

To meet high safety standards of current aviation , EASA decided to revisit the standard framework developed for conventional fixed-wing aircraft and helicopters with internal combustion engines, to tackle the new challenges due to the introduction of new technologies and new concepts of air transport. This effort led to the publication of the ”Special Condition for small-category VTOL aircraft” (Ref. 1). It applies to person-carrying VTOL heavier-than-air aircraft in the small category, with lift/thrust units used to generate powered lift and control. The small category covers aircraft with a passenger seating configuration of 9 or less.

To reach the appropriate flight safety the VTOL.2135 Controllability requires the aircraft to be ”controllable and manoeuvrable, without requiring exceptional piloting skills, alertness, or strength, within the operational flight envelope and must be controllable and manoeuvrable within the limit flight enve-

Phase of flight: CRUISE (Example)									
FltC $X_{FE} * X_{FC} * X_{AD}$	Atmospheric Disturbance (AD)								
	Light			Moderate			Severe		
	Flight Envelope (FE)								
Failure Condition (FC)	NFE	OFE	LFE	NFE	OFE	LFE	NFE	OFE	LFE
Nominal Condition	SAT	SAT	SAT	SAT	SAT	ADQ NOTE 1	SAT	ADQ NOTE 1	CON NOTE 1
Probable up to Remote Failure Conditions:	SAT	SAT	SAT	SAT	ADQ NOTE 1	CON NOTE 1	ADQ	CON NOTE 1	CON NOTE 1
Extremely Remote Failure Conditions:	SAT	ADQ	CON	ADQ	CON NOTE 1	NOTE 2	CON	NOTE 2	NOTE 2

NOTE 1: This is considered to be a transient condition, and it is expected that better HQR will be achieved when the AD level is decreased. Likewise it should be demonstrated that better HQRs are achieved in the more favourable Flight Envelopes: such transition should be relatively quick and without requiring exceptional piloting skills.

NOTE 2: This FC is shaded in red as it could possibly have a related probability lower than Extremely Improbable, and should not be considered. If the FC probability is greater than Extremely Improbable, then the minimum HQR should be CON.

Figure 1. Minimum Acceptable Handling Quality Rating, as described in (Ref. 2).

lope" (see (Ref. 1)).

To meet this requirement, EASA proposed as a means of compliance in MOC.VTOL.2135 (Ref. 2) the Modified Handling Qualities Rating Method (MHQRM) .The idea behind this proposal is that to demonstrate compliance to the stability, manoeuvrability and controllability, it is necessary to collect evidence on the vehicle HQ and so ensure that there is enough workload capability to operate the aircraft safely . The process described as MHQRM asks to verify for each phase of flight the achievement of a minimum level of HQ Rating depending on the level of atmospheric disturbances, the failure condition and the flight envelope considered (Ref. 2). The table is shown in Figure 1. For better understanding, the reader is referred to the original MOC document (Ref. 2)

This reopened the discussion about the usage of so-called Mission Task Elements (MTE) for civil certification (Ref. 3), which is a well-known concept introduced by the military specification ADS-33 (Ref. 4). EUROCAE developed a new guideline, ED-295 (Ref. 5), to collect evidence to complement the MHQRM, where MTEs are specifically developed for eVTOLs under the name of Flight Test Maneuvers (FTMs). Given the large number of conditions contained in Figure 1, some may present flight test safety challenges and other possible difficulties to be exactly replicated. The ED-295 explicitly says that " it is foreseen that simulation could in turn be used to collect further evidence [...]. These tests would be performed using pilot-in-the-loop simulation".

To achieve the goal of using simulation it is here proposed to follow the approach already outlined in the Rotorcraft Certification by Simulation (Ref. 6). It requires to first build the FSM in the Domain of Validation where the simulation can be compared with the results of flight tests. Within the validation process, it shall be assured that the errors are below the required tolerances and the uncertainties shall be assessed to evaluate the credibility of the simulation.

A similar approach will be followed in the current research, composed by the following steps:

1. Select for each FTM a set of Predicted HQs that will be used to validate the model
2. Identify the uncertainty of each simulation parameter
3. Assesses the error and the uncertainty of each Predicted HQ metric selected to ensure that the error is limited and the uncertainty is known.
4. Assess the impact of uncertainty in the simulation on the evaluation of HQ ratings.
5. Perform the FTM in the simulator to assess the HQ Rating considering the impact of uncertainty in this assessment.

The Predicted HQ, such as bandwidth, dynamic stability and attitude quickness, are used as fundamental indicators of the model's sufficiency for intended use, specifically for flight simulation trials based on a designated FTM. For certification purposes, the comprehensive approach to model fidelity assessment in both time and frequency domains, under the above-specified requirements, is deemed more robust than relying solely on time-domain matching. Additionally, using short maneuvers involving simple control inputs, such as step or doublet inputs, mitigates pilot-related factors and trajectory deviations over time. Initial tolerances for fidelity assessment are proposed based on CS-FSTD(H) (Ref. 7).

With the above-mentioned regulatory context in mind, the eVTOL industry will have to rely on flight simulation and analysis to propose flight test plans which are compatible with ambitious schedules. The MHQRM approach anticipates the collection of evidence for flight conditions accounting for failures and atmospheric disturbances in several areas of the aircraft's Flight Envelope. While this new approach strives to achieve high safety goals, it will require extensive flight testing. Additionally, for eVTOL designs unlike any other flying rotorcraft, engineers have no previous experience or flight data available, as is the case for the helicopter manufacturers. Consequently, there is a general recognition of the fact that a holistic approach is needed to better integrate flight simulation into the HQ certification process, as confirmed by (Ref. 3), (Ref. 6) and (Ref. 8). The current research aims to contribute to the development and widespread use of simulation for certification, which allows to reduce flight testing hours and fosters the proper use of simulation in making strategic decisions. The currently emerging eVTOL industry can greatly benefit from this approach in terms of time, costs and safety.

The primary aim of the current research is to develop a mid-fidelity rigid FSM of a small-scale lift+cruise eVTOL aircraft, which will be used to demonstrate how to build model credibility and show compliance with VTOL.2135 Controllability (Ref. 1) requirement by employing Certification by Simulation. This will be achieved by following the guidelines of RoCS (Ref. 6), as outlined above. This first paper will focus on the FSM development, leaving all aspects related to the development of an appropriate flight simulation system to provide appropriate cues to pilots at a later stage. Furthermore, the crucial aspect of assessing the impact of uncertainties of the model on the HQ Rating inferred through the usage of the flight simulator will not be tackled.

In the existing eVTOL simulator, the propeller loads are derived from wind tunnel testing results of an isolated propeller, while the aerodynamic loads on the fixed lifting surfaces are estimated using the methodology outlined in (Ref. 9). This methodology, however, does not account for the effects of propeller wake induction. As a result, it was deemed necessary to investigate the aerodynamic interference and evaluate whether its contribution to the overall aerodynamic loads should be considered. This paper presents preliminary results from the ongoing research, as described in the previous sections, which focus on the development of a mid-fidelity aerodynamic simulation capable of capturing aerodynamic interference—a phenomenon recognized as particularly challenging to model accurately at low speeds. For this purpose, the aerodynamic solver DUST, known for its versatility, is employed (Ref. 10).

Using the DUST aerodynamic model, a methodology for calculating stability derivatives as functions of attitudes and angular rates is developed. This data will be integrated into the existing low-fidelity Matlab+Simulink real-time model, required for the future piloted flight simulation. The DUST model is also intended to be directly integrated with MBDyn, a multi-body solver used for rotorcraft dynamic simulations, to enable nonlinear simulation of aerodynamic loads (Refs. 11,12). Through a comparative analysis of results from both models, a methodology will be formulated for physics-based tuning of the real-time model, based on insights from the mid-fidelity model. The use of Predicted HQ for fidelity assessment will serve as a valuable tool for evaluating the sufficiency of the FSM and verifying the applicability of ADS-33 (Ref. 4) requirements and CS-FSTD(H) (Ref. 7) tolerances for fidelity assessment.

EVTOL DESCRIPTION

The small unmanned eVTOL under investigation was designed and manufactured by the Aerospace Systems and Control Laboratory (ASCL) of the Department of Aerospace Science and Technology at the Politecnico di Milano (DAER) (Ref. 13) and is depicted in Figure 2 and 3. It utilizes 8 three-bladed propellers for vertical lift, each operating with variable RPM and fixed pitch. In helicopter mode, the aircraft is controlled through the differential thrust of all vertical propellers. For horizontal thrust, the aircraft is equipped with 2 two-bladed propellers. The fuselage is reduced in size to contain the batteries and necessary avionics, the wings are rectangular without twist while the empennage is H-shaped. The main geometry and mass properties of the eVTOL are detailed in Table 1. The eVTOL center of gravity is located in its vertical plane of symmetry and at 25% of the wing chord. Figure 2 shows propeller numbering convention and their direction of rotation. This system has the scale of a drone and not the scale of an eVTOL capable of carrying passengers. However, it has been considered a valid benchmark for this research, since it resembles a typical lift + cruise eVTOL configuration.

While it would have been possible to scale up the configuration to obtain a passenger-carrying vehicle, it has been chosen to keep the current scale to allow for a direct comparison of simulation results with experimental tests.

Table 1. eVTOL Characteristics.

Parameter	Value	Unit
Max Gross Weight W_{TO}	7.1	kg
Center of gravity x_{CG}	0	m
Wing and fuselage span b_W	3	m
Wing chord c_W	0.26	m
Wing incidence i_W	4.5	deg
Fuselage span b_F	0.42	m
Horizontal stabilizer span b_{HT}	0.721	m
Horizontal stabilizer chord c_{HT}	0.13	m
Horizontal stabilizer arm x_{HT}	1.08	m
Horizontal stabilizer incidence i_{HT}	0	deg
Vertical propeller diameter d_{prop}	0.178	m
Vertical propeller chord at 80% r c_{prop}	0.0124	m
Forward propellers y-coordinate l_f	0.1815	m
Rearward propellers y-coordinate l_r	0.1415	m
1st row of propellers x-coordinate l_1	0.6	m
2nd row of propellers x-coordinate l_2	0.33	m
3rd row of propellers x-coordinate l_3	0.33	m
4rd row of propellers x-coordinate l_4	0.6	m

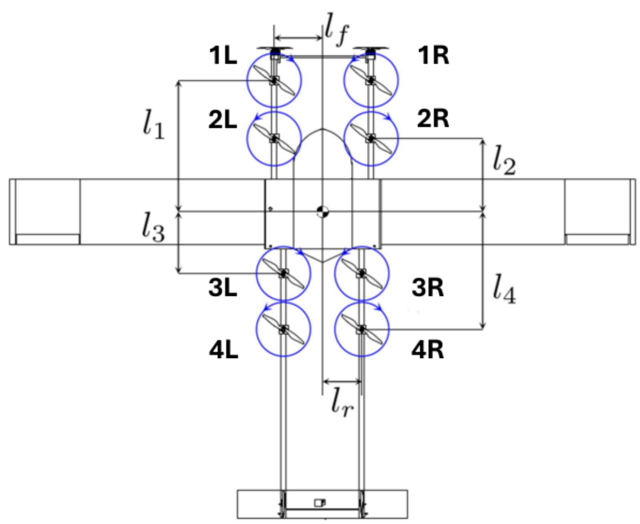

Figure 2. eVTOL configuration and propeller rotation direction.

NUMERICAL MODELS DESCRIPTION

DUST Aerodynamic model description

For the aerodynamic modeling, a computational tool called DUST developed by Politecnico di Milano, was used. DUST is an open-source software which allows for modeling of solid bodies as thick surface panels, thin vortex lattice elements,

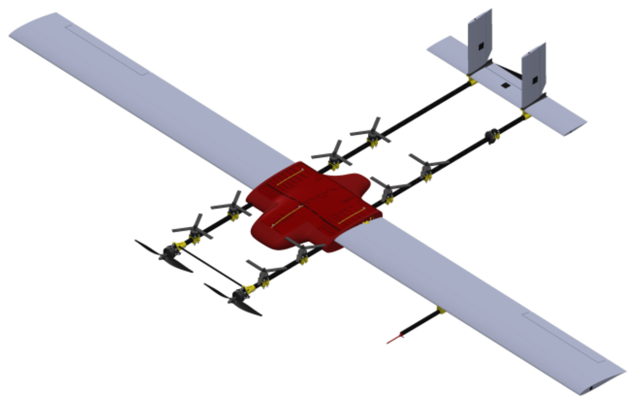

Figure 3. eVTOL overview.

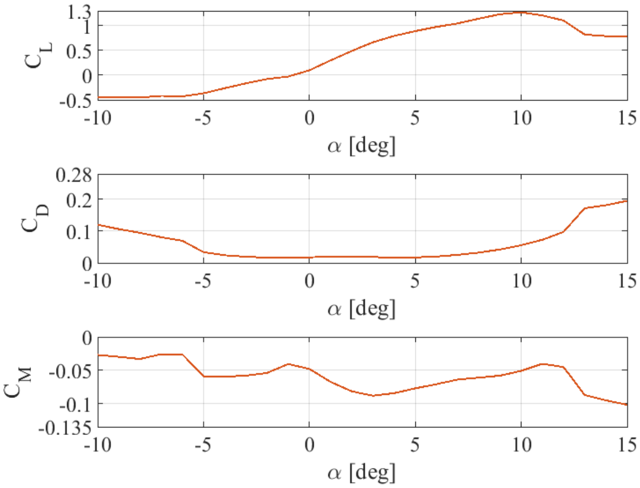

Figure 4. Aerodynamic characteristics of wing airfoil Selig 2046 at Re $= 80,000$ **and Ma** $= 0.1$**.**

Table 2. Reynolds numbers for all eVTOL components at $U_\infty = 6$ **m/s.**

Component	Re
Propeller blade at 80% r	865,000
Wing and fuselage	86,000
Horizontal tail	43,000

and lifting line elements. A Vortex Particle Method (VPM), which provides a Lagrangian description of the free vorticity field in the wake, was implemented for the wake modeling. Details about the mathematical formulation of the solver can be found in (Ref. 10). The aforementioned features of DUST make it suitable for the investigation of aerodynamic interactions between multiple propellers and propeller wakes with fuselage and wing, on a fraction of the computational cost of CFD methods. DUST aerodynamic model is used to identify the appropriate methodology for calculating stability derivatives as functions of attitudes and angular rates.

Following a systematic building-block approach, the propeller geometry was extracted from the off-the-shelve purchased propeller through 3D scanning, and a single fixed-pitch three-bladed propeller model in DUST was developed, using lifting line elements. The propeller rotational speed was set to 1500 rad/s for all simulations, which corresponds to the required propeller thrust at 6 m/s horizontal velocity. For the fixed lifting surfaces, vortex lattice elements with aerodynamic tables correction were used. All airfoils aerodynamic characteristics were obtained using Xfoil viscous calculation, to account for the low maximum lift coefficient and early stall at low Re. The Reynolds numbers are summarized in the Table 2. The example of aerodynamic characteristics of the wing airfoil Selig4026 at Re $= 80,000$ are shown in Figure 4.

For the fuselage the following modeling approaches were investigated:

1. As a bluff body which allows only for potential flow calculation. This approach does not allow for fuselage wake shedding as the fuselage has no trailing edge, therefore the aerodynamic loads are highly underestimated.

2. As a lifting surface with variable chord, to reflect the fuselage shape, with ellipse aerodynamic characteristics assigned to the cross-sections, see Figure 5. This method allows for fuselage wake shedding, but there is still wing lift loss at the root due to the different angles of incidence of the wing and the fuselage. In addition, there are convergence issues of the nonlinear VLM for this geometry.

3. As a lifting surface with constant chord, equal to wing chord, and equal incidence angle (see Figure 6). Ellipse characteristics were offset to account for the angle of attack.

4. Fuselage geometry is modelled as identical to the wing, which leads to the overestimation of the lift on the fuselage and wing but balances the pitching moment distribution.

Figure 7 and Figure 8 compare the vertical force and pitching moment distribution along the fuselage and wing for the above-mentioned modelling approaches.

The last and the simplest modelling approach was chosen, motivated by the balanced pitching moment, which plays a crucial role in longitudinal stability, and due to other modelling approaches convergence issues using the nonlinear vortex lattice method at negative angles of attack. Besides, continuous wing facilitates the interpretation of the results for the load cases with the propellers, as there is no effect of fuselage-wing discontinuity on the flow field which superimposes on the propellers wake induction. The investigation of different fuselage modeling approaches gave an insight into introduced uncertainty, while the final choice of the most accurate modelling approach can be made by having experimental results or an accurate CFD analysis.

Finally, the complete eVTOL geometry was constructed using the DUST pre-processor. The generated geometry of the full configuration is shown in Figure 9. The origin of the body

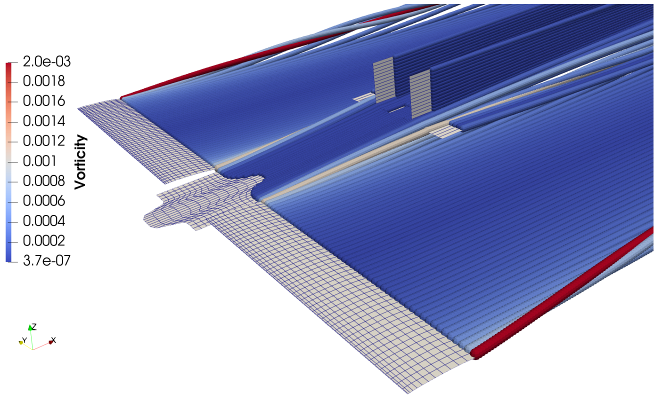

Figure 5. Visualisation of eVTOL fuselage modelling approach 2 and wing wake vorticity.

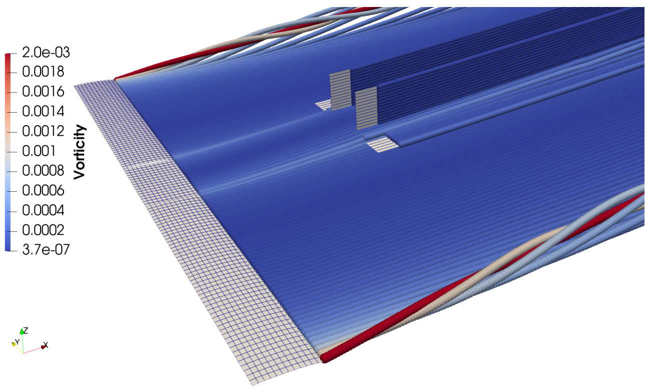

Figure 6. Visualisation of eVTOL fuselage modelling approach 3 and wing wake vorticity.

system of coordinates is placed in the eVTOL vertical plane of symmetry and in the wing 25% chord.

Stability derivatives calculation methodology

Longitudinal static stability derivatives $C_{L\alpha}$, $C_{D\alpha}$ and $C_{M\alpha}$ and longitudinal forces and moments coefficients, C_L, C_D and C_M, were obtained by performing a time marching simulation with $U_\infty = 6\frac{m}{s}$ at different vehicle angle of attack and the integral loads were extracted at the end of the simulation, for the configuration without the propellers, or mean values of loads were calculated for the full configuration with the propellers.

Dynamic stability derivatives for pitch rate, C_{Lq} and C_{Mq} were calculated based on the methodology developed in (Ref. 14), by imposing a sinusoidal oscillatory pitching motion to the eVTOL in the configuration without the propellers or in full configuration. The main assumption underlying the stability derivatives computation methodology is that the aerodynamic forces and moments acting on the aircraft are linear with respect to both the angle of attack α and pitching rate q variations. According to the single point method whose foundations are described in (Ref. 14), the dynamic stability derivative, in the form of a coefficient function of angle of attack, can be expressed as follows:

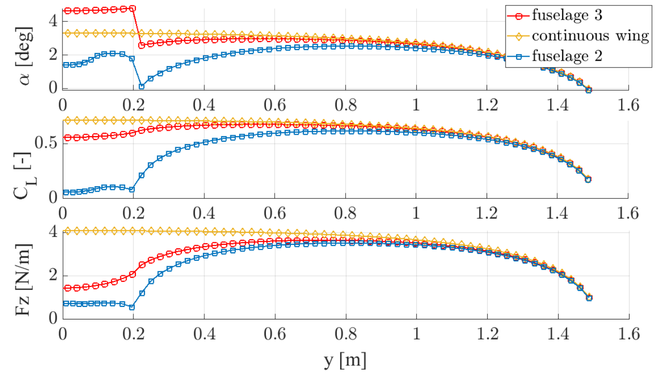

Figure 7. Angle of attack, C_L and F_z distribution along the fuselage and wing – comparison between different modelling approaches.

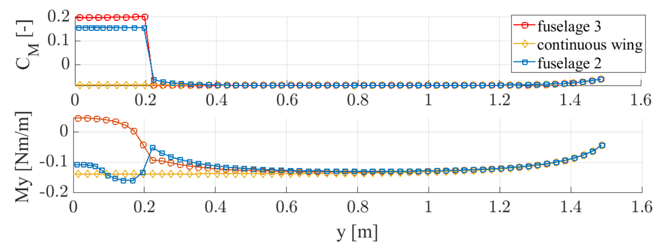

Figure 8. Angle of attack, Cm and My distribution along the fuselage and wing – comparison between different modelling approaches.

$$c_{jq} = \frac{\Delta c_{jq}(t)|_{t=t_{\alpha_0}}}{\alpha_A k} \tag{1}$$

$$k = \frac{c_W q}{2U_\infty} \tag{2}$$

where:

α_A - amplitude of angle of attack for pitching oscillation
k - reduced frequency
q - pitch rate

$\Delta c_{jq}(t)|_{t=t_{\alpha_0}}$ corresponds to the operation of measurement of the thickness of the aerodynamic force or moment hysteresis ellipse around α_0 (see Figure 10).

RESULTS AND DISCUSSION

Isolated propeller performance in forward flight

Isolated propeller performance at the horizontal velocity of 6 m/s and inflow angle of 0 deg is given in this section for reference. The mean value of thrust obtained is 8.4 N for a rotational velocity of 1500 rad/s. The H-force with respect to the propeller axis of rotation is found to be 0.18 N. Figure 11 shows the isolated propeller thrust in time, comparing the raw and filtered signals. The bottom plot shows the Fast Fourier Transform of propeller thrust, highlighting significant

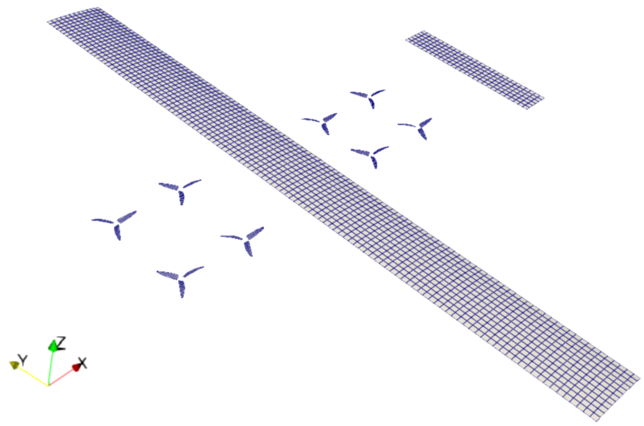

Figure 9. eVTOL full configuration created in DUST pre-processor.

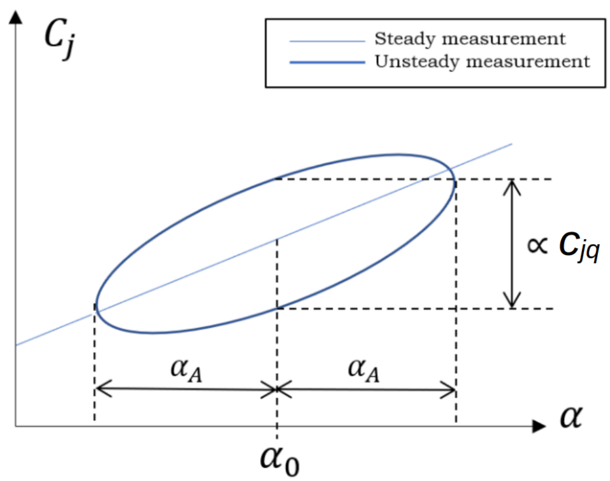

Figure 10. Graphical representation of the extraction of the dynamic derivative, adapted from (Ref. 14).

frequency components at the propeller's first (3/rev) and second (6/rev) transmission harmonics. This indicates that the thrust contains periodic components related to the propeller's blade rotational frequency.

The time step imposed for the propeller simulation is 0.1164 ms which corresponds to 10 deg of propeller rotation. The author is aware that it is a relatively big time step and it was verified that a time step corresponding to 5 deg provides lower results for thrust by 0.2 N (2.4%). However, the high rotational speed of propellers and the low horizontal speed introduce a difference in time scales of approximately 20 times, between rotating lifting surfaces (0.1164 ms) and fixed lifting surfaces (2 ms). In order not to compromise the already long computational times (ca 12 h on a commercial laptop for a static simulation of the full configuration), a trade-off was made and the time step corresponding to 10 deg was chosen. The resulting propeller's thrust uncertainty will be considered in future work.

The flow field around the isolated propeller is unsymmetrical,

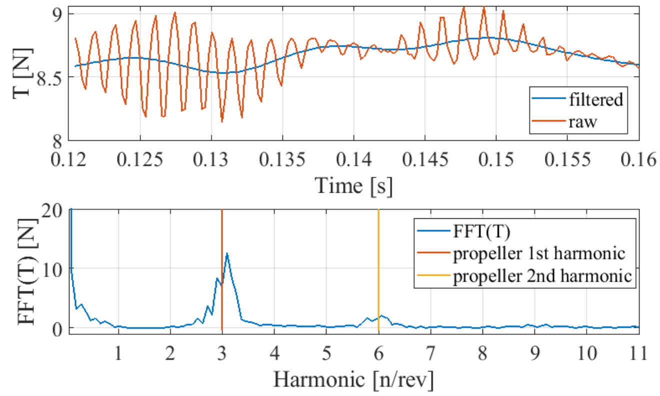

Figure 11. Isolated propeller thrust in time and frequency domain, expressed as a function of the number of periods per rotor revolution.

which is visible in the Figure 12 representing the induced velocity and velocity magnitude field just above the propeller, averaged over the time of the simulation. The propeller with a clockwise rotation direction accelerates the flow to the right side and upwards. This is because the blades are rigidly mounted on the mast, preventing any flapping movement and the resulting load redistribution, as it occurs with articulated rotors. The loads on the advancing and retreating blades differ significantly, as shown in Figure 13.

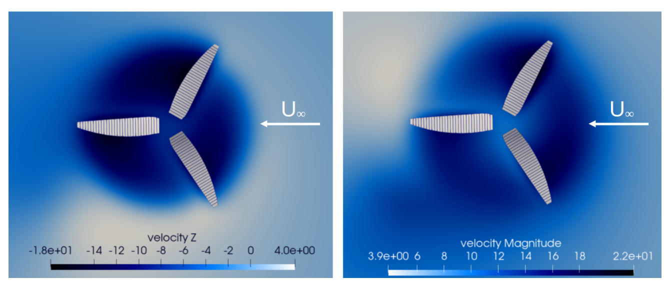

Figure 12. Isolated propeller instantaneous induced velocity and velocity magnitude flow field (clockwise rotation).

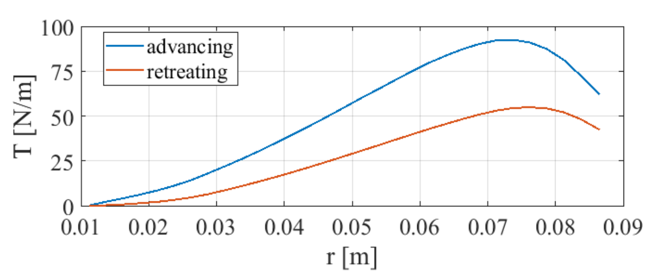

Figure 13. Isolated propeller advancing and retreating blade thrust distribution.

Propeller-propeller aerodynamic interference

To investigate the presence of propeller-propeller induction, propeller loads for a full configuration were calculated. The horizontal velocity for this flight condition is 6 m/s and the vehicle angle of attack is 0 deg. First, the frequency contents of the first and second propeller thrust were examined, in the simulation range when the propeller's wakes are mixing. The top plot in Figure 14 shows the first propeller lift in time, comparing the raw and filtered signals. The bottom plot shows the frequency content of the force signal, highlighting significant frequency components at 3/rev and 6/rev harmonics.

The second propeller lift force in the frequency domain, see Figure 15, reveals different behaviour for the first propeller. The visible peaks are still at the first and second propeller main transmission harmonics, but the first peak is noticeably higher and the entire frequency content appears more scattered, indicating the presence of aerodynamic interactions with the first propeller. The rear pair of propellers manifests similar behaviour.

Next, mean values of thrust for 0 deg angle of attack are presented in Figure 16, to compare values of mean thrust for each propeller with an isolated one.

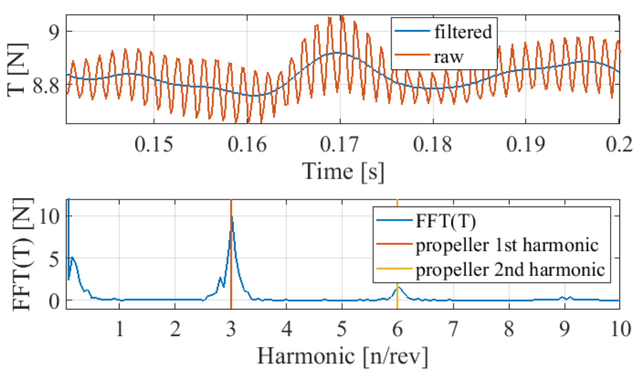

Figure 14. First propeller thrust in time and frequency domain.

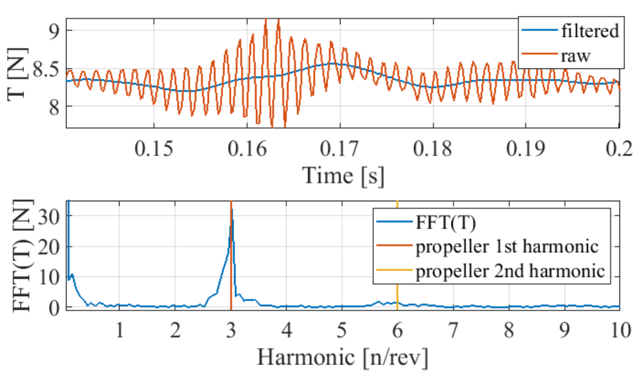

Figure 15. Second propeller thrust in time and frequency domain.

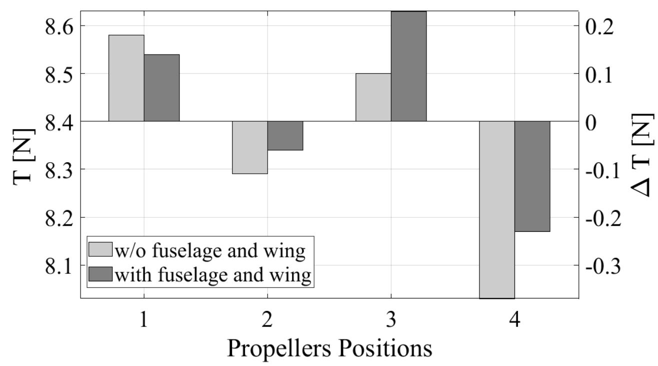

Figure 16. Propellers thrust comparison, $U_\infty = 6$ m/s, $\alpha = 0$ deg.

The thrust of the second and fourth propeller is lower due to the proximity of the first and third propeller respectively. This trend is visible for both cases with and without fixed lifting surfaces. The same behaviour is observed for different angles of attack but was not shown on the graph for clarity. It was also revealed that the first and third propeller thrust is somewhat higher than that of the isolated one. It could be possible due to the induction of the second or fourth propeller on the first and third propeller respectively. Overall, the computed thrust values lie approximately within $+/-0.2$ N tolerance with respect to the isolated propeller thrust which corresponds to $+/-1\%$ of the throttle for this flight condition.

The simulation case without the wing was intended to verify if there is a noticeable induction of fuselage and wing on the propeller loads. From the available result, it can be observed that the third and fourth propeller thrust values for the case with the fuselage are noticeably higher then the case with no fuselage (approximately by 0.1 N), which could be considered evidence of how the presence of fuselage and wing influences the propellers wakes.

Loads time histories for simulations with propellers

In this section, an example of raw data of loads time histories of static simulations at $U_\infty = 6$ m/s and $\alpha = 6$ deg obtained for the eVTOL configuration with propellers is discussed (see Figures 17 and 18). The load time histories for the simulation with propellers have high variations, in particular the pitching moment, and it is difficult to extract steady loads. There are extended ranges where the calculations do not converge (see times 1.01 and 1.06 s). This occurs when the simulation starting vortex particles of the first two rows of propellers approach the wing and the fuselage, and when the calculation of loads on fixed lifting surfaces does not converge due to the turbulent flow around them. Therefore the exact values are to be treated with caution and for a quantitative analysis an approach shall be developed to account for the load uncertainty. The time range of $0-1$ s of the simulation is dedicated to wing wake generation without the propellers. It was achieved by running the static simulation in full configuration with the propellers moved outside of the simulation domain.

To continue the simulation with the propellers, the simulation was restarted by modifying the propellers' reference frame to their correct position. This operation allowed us to reduce the computational time to 12 hours on a commercial laptop. The wake of the fourth row of the propellers reaches the horizontal tail at 1.08 s (see peaks appearing in the pitching moment of the horizontal tail, which indicates minimum simulation time). Afterwards, the horizontal tail moment is highly unsteady due to the interference with the propellers' wake, but its mean value, calculated for the time range $1.16-1.2$ s, can be qualitatively compared with the case without the propellers. Next, the analysis of mean loads for all simulated angles of attack is presented.

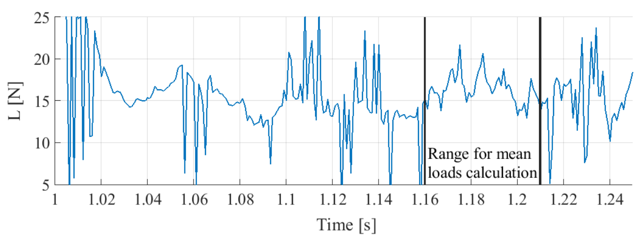

Figure 17. Raw data of lift time history, $U_\infty = 6$ m/s, $\alpha = 6$ deg.

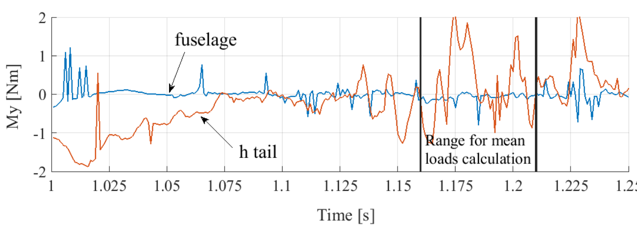

Figure 18. Raw data of pitching moment time history, $U_\infty = 6$ m/s, $\alpha = 6$ deg.

Propellers induction on fuselage and wing

This subsection analyses the propellers' induction on fuselage and wing loads at angles of attack ranging from -5 to 6 deg, by comparing them with loads for configuration without the propellers' induction, for angles of attack from -6 to 8 deg. The range of studied angles of attack is limited by the model convergence and is smaller with the propellers with respect to the range without the propellers. No horizontal stabilizer loads are included since they will be discussed in the following section. The propellers' loads are not discussed in the subsequent analysis, since they were discussed in the previous section. The fuselage and wing loads are shown in Figure 19. The angle of attack is defined with respect to the eVTOL longitudinal axis. The wing is mounted on the fuselage with an incidence angle of 4.5 deg and the wing profile produces zero lift at ca -0.8 deg, therefore the zero lift for the configuration without the propellers is at about -6 deg. At the same angle also the minimum wing drag is visible. The pitching moment is negative, except for the angle of attack of -6 deg. For the configuration with the propellers, a lift increment is visible for negative angles of attack and lift loss for positive angles of attack. Pitching moment values change due to the altered flow around the fixed wing surfaces, but a detailed analysis cannot be conducted using only average loads plots. To interpret the nature of propeller induction, the velocities and load distributions along the fuselage and wing span for negative and positive angles of attack are analyzed. No detailed analysis for drag will be done due to the very low values, but it can be considered in the uncertainty assessment.

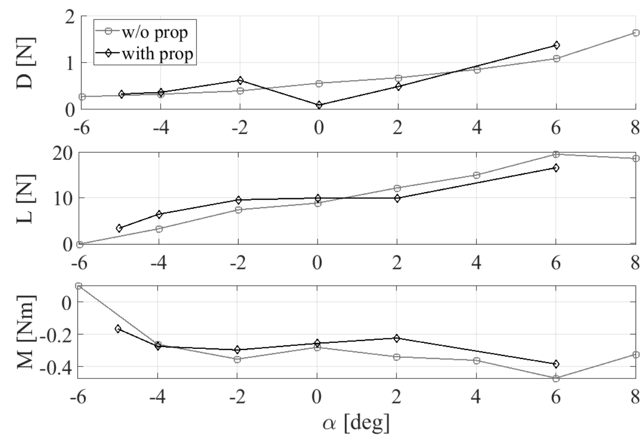

Figure 19. Lift and pitching moment of fuselage and wing with and without propellers induction, and without horizontal stabilizer loads.

Figure 20 presents local inflow velocity at the fuselage and right wing for $\alpha = 6$ deg. V_{2d} is the magnitude of a sum of the free stream velocity and influence of the wing and propeller downwash, projected on the airfoil plane and is measured at the 75% chord, according to (Ref. 15). U_{px} is its component which lies along the airfoil chord and is positive when directed rearwards, and U_{pz} is its component perpendicular to the airfoil chord, positive when directed upwards. The forward propellers' location is at 0.181 m and the external blade tip at 0.271 m. Propellers' influence is generally visible until y = 0.6 m. V_{2d} is reduced, at the fuselage to $4-5$ m/s, at the wing $5-6$ m/s. U_{pz} multiple peaks of velocity perpendicular to the wing chord are visible indicating the presence of propeller wake.

Next, the effective angle of attack, lift and pitching moment are shown in Figures 21 and 22. According to (Ref. 15), the effective angle of attack of the in-plane relative velocity at the control point is corrected with the 2D influence needed by formulation developed in (Ref. 16), to get the right angle of attack to be used in the aerodynamic tables:

$$\alpha_{EFFi} = \alpha_{pi} - \alpha_{Di} \tag{3}$$

$$\alpha_{Di} = \alpha_{3Di} - \alpha_{2Di} \tag{4}$$

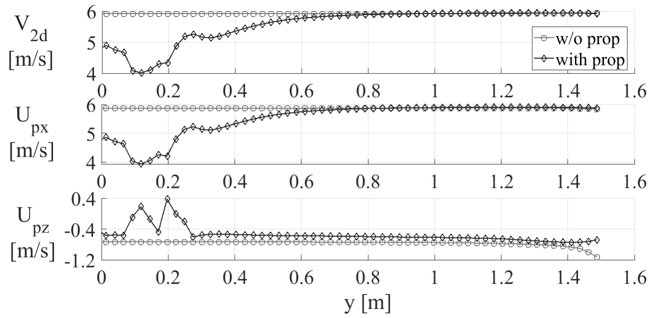

Figure 20. Local inflow 2d velocity at the fuselage and wing and its vertical and horizontal components — distribution along the fuselage and wing span, $\alpha = 6$ deg.

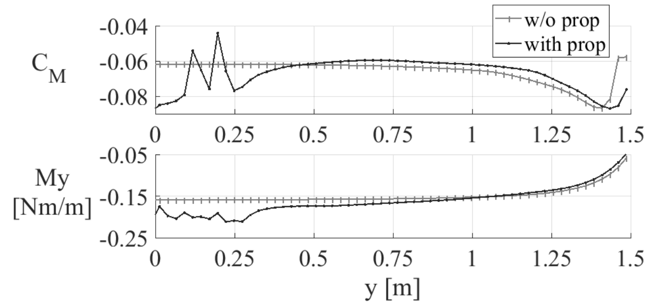

Figure 22. Pitching moment coefficient and pitching moment distribution along the fuselage and wing span, $\alpha = 6$ deg.

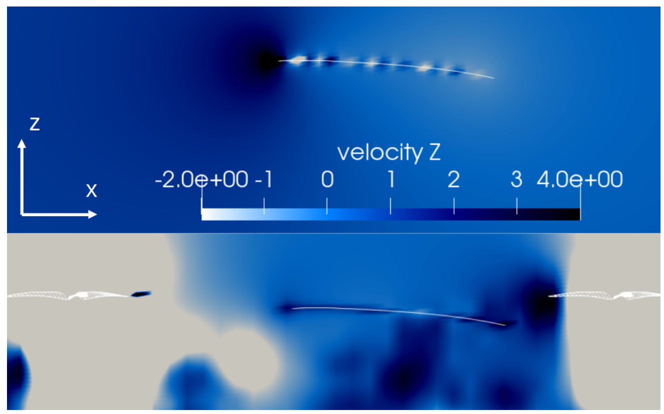

Figure 23. Visualization of vertical velocity around the wing. Upper figure – isolated fuselage and wing, lower figure – full configuration with propellers.

where: α_{pi} is the pitch angle, α_{Di} is the downwash angle, α_{3Di} is the total three-dimensional downwash angle, α_{2Di} is the equivalent two-dimensional downwash angle.

Loads are given in the wing local reference frame with x axis along the wing chord directed rearward, and are averaged in time ($0.16 - 0.2$ s of the simulation). Effective angle of attack increments due to peaks in U_{pz} are still visible and lead to a local stall of the fuselage and wing. However, the dominant effect on lift and pitching moment is due to the reduction of the velocity magnitude V_{2d}, which leads to the loss of lift and the increase of the pitching moment absolute value in the proximity of the propellers. The behaviour of all quantities of interest on the left wing and left portion of the fuselage is the same and was not reported for simplicity.

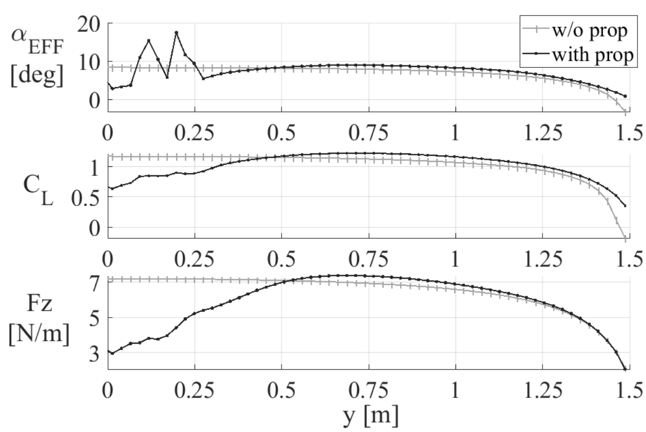

Figure 21. Angle of attack, lift coefficient and lift distribution along the fuselage and wing span, $\alpha = 6$ deg.

This behaviour can be explained through a visualization of the flow around the wing. In Figure 23 the aerodynamic interference between the propellers and fuselage is visualized through the vertical velocity. The cross-section is made at span $y = 0.1815$ m, in the front right propeller axis of rotation. At the wing leading edge, the upward circulation of the flow is significantly reduced, while at the trailing edge, an upward velocity component arises due to the interference with propeller blade tip vortexes shed by the third propeller.

Next, the load distribution along the wing and fuselage for $\alpha = -4$ deg is discussed. Figure 24 presents local inflow velocity at the fuselage and right wing for $\alpha = -4$ deg. V_{2d} and U_{px} change along the span until ca 0.5 m, with a minimum value of 5.3 m/s, and a maximum of 7.2 m/s. With the propellers, U_{pz} absolute value increases to -1.88 m/s (without the propellers -0.65 m/s) and returns to baseline at ca 0.28 m. Note that for negative angles of attack, the U_{pz} modification due to third propeller wake induction is negative (induced velocity downwards), while for the positive angles of attack, it is positive (induced velocity upwards). This suggests that the mechanism of the propeller induction on the fuselage and wing might be very sensitive to the angle of attack. To fully understand this further analysis is needed.

The effective angle of attack along the fuselage (see Figure 25) span is reduced from 0 deg to -10 deg due to U_{pz} alterations discussed above, but along the wing span its value becomes positive. This increment produces additional lift at the wing, which compensates for the lift loss at the fuselage (see Figure 19). Additionally, the pitching moment absolute values are increased along the wing (nose-down, see Figure 26). This suggests upwards induced velocity at the wing trailing edge which contradicts the negative values of U_{pz}.

To summarize, for both negative and positive angles of attack

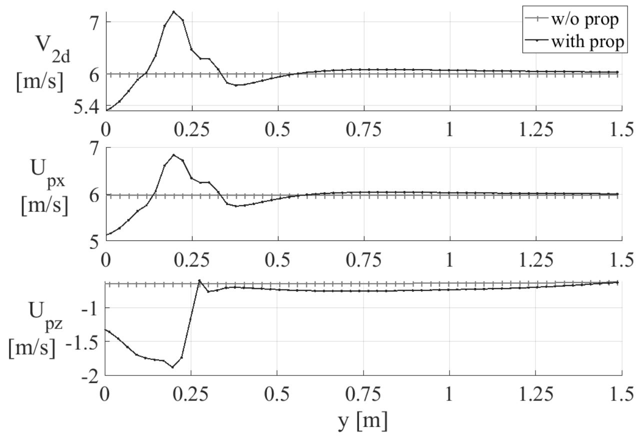

Figure 24. Local inflow 2d velocity at the fuselage and wing and its vertical and horizontal components — distribution along the fuselage and wing span, $\alpha = -4$ deg.

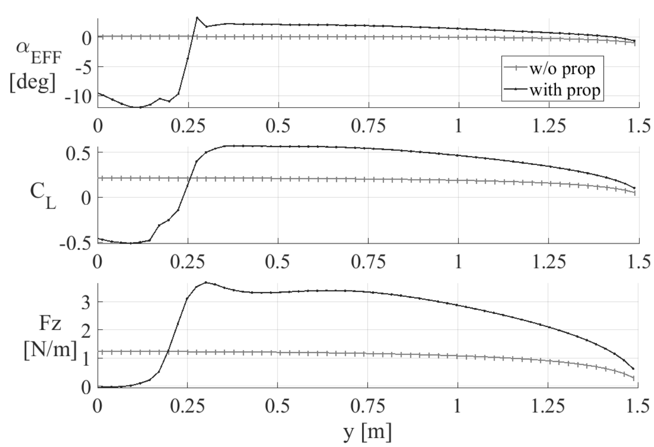

Figure 25. Angle of attack, lift coefficient and lift distribution along the fuselage and wing span,$\alpha = -4$ deg.

lift loss is observed along the fuselage and inner portion of the wing distribution, but due to different behaviour of local velocities. For positive angles of attack, the effective angle of attack on the wing is not changed, while for negative angles of attack, the effective angle of attack becomes positive which leads to a lift increase. The reason for that is not clear and must be further investigated.

For the positive angles of attack, the lift loss at the fuselage is $2.25-3$ N and would require the overall throttle reduction of 1.5 % on all propellers.

Propellers induction on horizontal stabilizer

In this section, the induction of propellers wake on horizontal stabilizer is discussed. Figure 27 presents horizontal stabilizer lift and pitching moment with respect to 25% wing chord, for configuration with and without the propellers. Horizontal stabilizer has a symmetric airfoil NACA0008 and 0 deg incidence, hence zero lift is produced at about 0 deg angle of

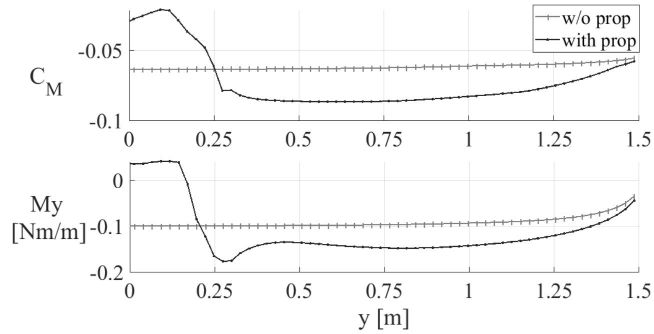

Figure 26. Pitching moment coefficient and pitching moment distribution along the fuselage and wing span, $\alpha = -4$ deg.

attack, without the propellers induction. For positive angles of attack, the horizontal tail produces a pitching-down moment, while for negative angles of attack pitching-up moment is produced. In the lift curve, a decrease of lift is observed for the range of 4 and 6 deg which is due to maximum aerodynamic interference with wing wake. In fact, for the isolated horizontal stabilizer and angle of attack of 6 deg the calculated lift is 0.9 N (w.r.t. 0.38 N) and the pitching moment is -1 Nm (w.r.t. -0.43 Nm). The interference of the horizontal stabilizer with the wing wake is less visible for negative angles of attack (values for -4 deg: L: -0.54 N, M: 0.62 Nm). Interference with the propeller's wakes introduced an offset in the horizontal tail lift and moment — negative offset for lift and positive offset for pitching moment (nose up). The interference is visible for the entire range of studied angles of attack.

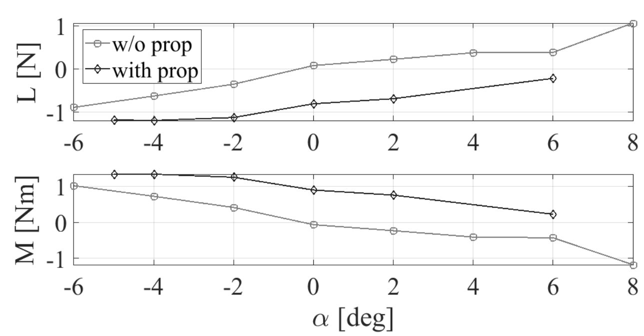

Figure 27. Horizontal stabilizer lift and pitching moment — without the propellers and with the propellers.

The propeller's induction is visible in Figures 28 and 29 which present the distribution of quantities of interest along the horizontal stabilizer span, for $\alpha = -4$ deg. V_{2d} for the case with the propellers is lower than the baseline and not regular along the span. U_{pz} changed significantly and reaches up to -1.75 m/s (in comparison to baseline -0.33 m/s in the middle of the horizontal stabilizer). As a result, the effective angles of attack are highly negative (max -15 deg w.r.t baseline -3.5 deg) and the horizontal stabilizer is stalled. Again the effect of propeller's induction manifests in the vertical force F_z relative negative increment and hence the tail pitching moment increment (nose up). The same behaviour was observed for positive angles of attack.

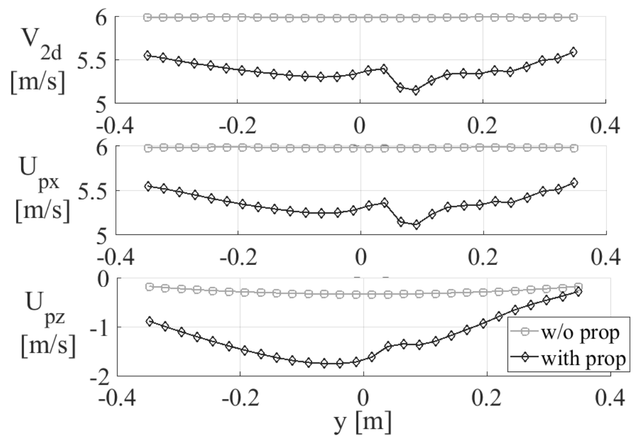

Figure 28. Local inflow 2d velocity at the horizontal stabilizer and its vertical and horizontal components — distribution along the horizontal stabilizer span.

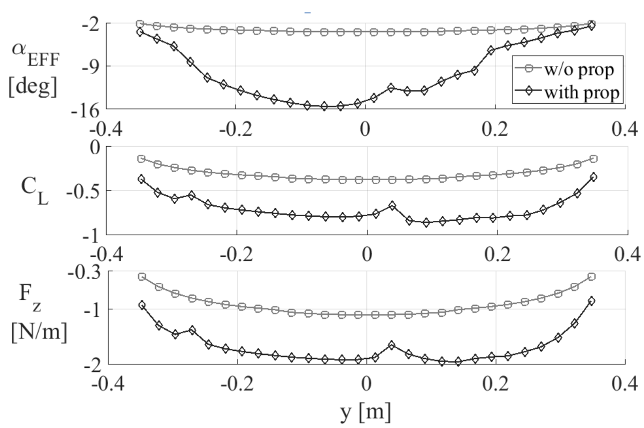

Figure 29. Angle of attack, lift coefficient and F_z distribution along the horizontal stabilizer span.

To balance the horizontal stabilizer pitch-up moment contribution which arose solely from the propeller's induction, a thrust increment is needed for the first and third propellers, while the thrust of the second and fourth propellers shall be reduced. This pitching moment contribution, calculated for the studied velocity 6 m/s is up to 1 Nm (see M_y offset in Figure 27), which results in required thrust compensation of about ± 0.93 N for each propeller to maintain static equilibrium. This is, so far, the most important contribution of propellers' induction on fixed-wing loads and shall be included in the modelling.

Aerodynamic interference influence on throttle values

To account for the additional loads arising due to aerodynamic interference of the propellers with wing and horizontal tail, thrust values on all propellers must be adjusted to maintain static stability. To account for propeller-propeller interference in the existing flight simulator, where the propellers are modelled as isolated by assigning an identical experimental thrust-throttle curve to each propeller, a correction factor will be added to each curve, to account for lift change based on propeller position. Figure 30 gathers all estimated aerodynamic interferences in terms of required thrust correction. The thrust correction was taken from the linear range of the experimental thrust-throttle curve, where 0.22 N of produced thrust corresponds to 1% of the throttle.

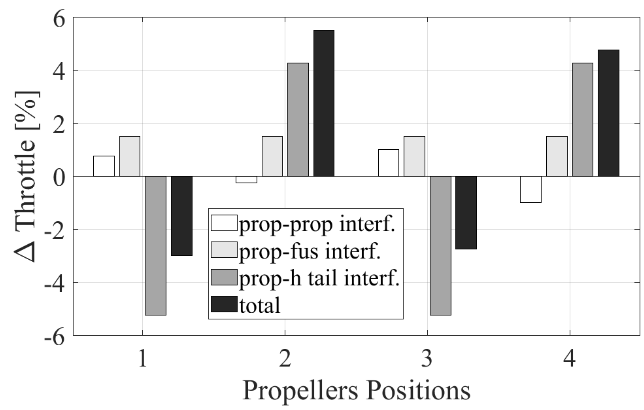

Figure 30. Required throttle contributions to account for aerodynamic interference.

The first and third rows of propellers require a negative throttle adjustment of approximately 3% due to the opposing effects of propeller-horizontal tail interference and other interferences. In contrast, the second and fourth rows of propellers require a significant positive throttle adjustment of around 5% due to the combined effects of propeller-horizontal tail interference and fuselage lift loss. The contribution of propeller-propeller interference is the least significant. Overall, the total throttle adjustments indicate that interference effects vary significantly by propeller position, with propeller-horizontal tail and fuselage interferences being the most influential.

Considering the requirement from FSTD(H) (Ref. 7), which imposes $\pm 5\%$ tolerance on the collective control position for low airspeed handling qualities, the modelling without aerodynamic interference between the eVTOL components, might lead to simulation thrust values which lie beyond the tolerance. This conclusion encourages considering the aerodynamic interference in the modelling, to build model credibility and assure that it is fit for the intended usage.

Dynamic stability derivatives for configuration without propellers

Dynamic stability derivatives with respect to pitch rate, C_{Lq} and C_{Mq} were calculated by imposing a sinusoidal oscillatory pitching motion to the eVTOL, about the body reference frame with its origin at 25% of wing chord, in the configura-

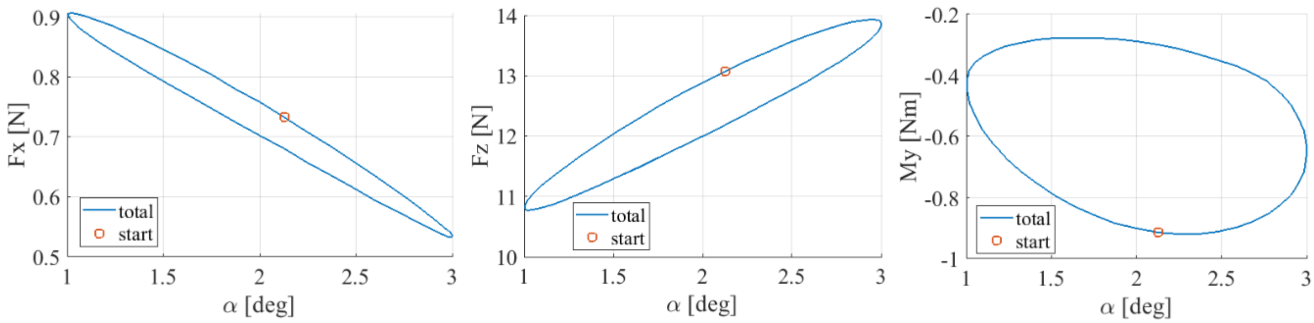

Figure 31. Loads hysteresis for a pitching oscillation, $\alpha_A = 1$ deg, $\alpha_0 = 2$ deg, without the propellers.

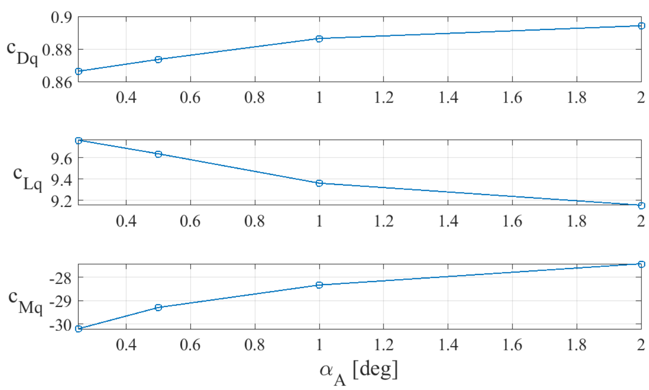

Figure 32. Dynamic derivatives vs. pitching oscillation amplitude, f = 1 Hz, $\alpha_0 = 2$ deg, without the propellers.

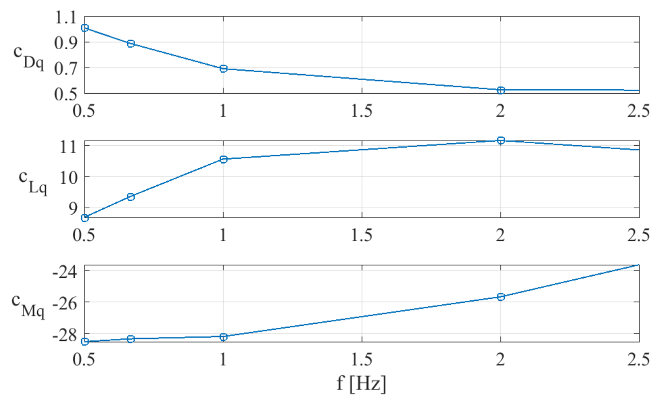

Figure 33. Dynamic derivatives vs. pitching oscillation frequency, $\alpha_0 = 2$ deg, $\alpha_A = 1$ deg, without the propellers.

-tion without the propellers. Figure 31 presents loads hysteresis for a pitching oscillation of an amplitude $\alpha_A = 1$ deg about the mean angle of attack $\alpha_0 = 2$ deg.

Subsequently, a sensitivity study on the dynamic derivatives was conducted to examine their dependence on oscillation amplitude and frequency. The results of this study are presented in Figure 32 and Figure 33 respectively.

The results indicate that the dynamic derivatives appear dependent on both the amplitude and frequency of the pitching oscillation. The solution appears to become amplitude-independent at larger amplitudes, but this is constrained by the narrow range of angles of attack due to early stall at low Reynolds number. The frequency dependency, however, shows no clear convergence. The effect of removing the horizontal stabilizer was also investigated to determine whether the observed non-linearity was due to aerodynamic interference. This analysis revealed a significant frequency dependency for the pitching moment, obviously since the pitching moment is produced mostly by the horizontal stabilizer. Linearizing the airfoil lift curve (see Figure 4) in the range of $0-10$ degrees also did not eliminate the dependency of the derivative C_{Lq} on frequency. Figure 34 presents the results for the configuration without the horizontal stabilizer and with a linearized airfoil lift curve. The obtained values were compared with the ones found in (Ref. 17) and were confirmed to be acceptable.

The reason for the strong dependency of dynamic derivatives on frequency for an isolated wing remains unclear. This suggests that a large number of simulations must be conducted to account for different frequencies when using the current methodology. Therefore, the methodology for calculating the dynamic derivatives may require revision.

CONCLUSIONS

This paper presents preliminary results of the development of an aerodynamic model of a small-scale lift+cruise eVTOL aircraft, to be integrated into a FSM intended to be used for HQ assessment assessment.

The main challenges encountered were as follows:

- Issues related to nonlinear VLM convergence for complex geometries;
- The small time scale necessary to compute correctly the aerodynamic loads of rotating lifting surfaces, due to high rotational speed and resulting in significant computational effort;
- A limited range of angles of attack for aerodynamic characteristics of the airframe due to low Reynolds numbers;

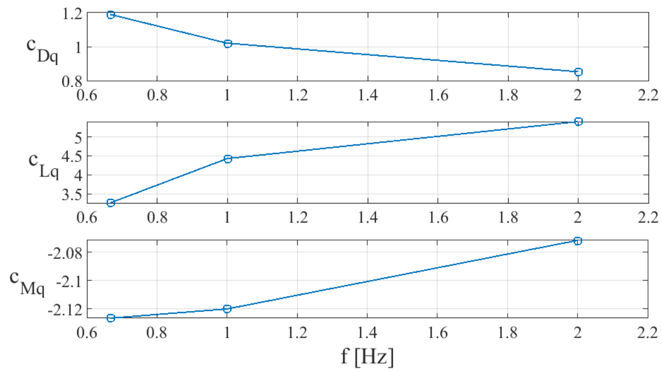

Figure 34. Dynamic derivatives vs. pitching oscillation frequency, $\alpha_0 = 2$ deg, $\alpha_A = 2$ deg, configuration without the horizontal tail, without the propellers.

- Unsteady loads on the fixed lifting surfaces caused by propeller wake interference, leading to difficulties in data interpretation;
- The need to perform a large number of simulations due to the dependency of dynamic derivatives on frequency.

The following phenomena and modeling methodologies were studied:

- The influence of the fuselage modeling approach on fuselage and wing loads was investigated. The simplest modeling approach, representing the fuselage as part of the main wing was chosen due to its best representation of the pitching moment and convergence. However, the overestimation of lift on the fuselage will need to be accounted for in the in the employment of the results in the FSM.
- The simulations revealed visible propeller-propeller interference, resulting in increased lift for the first and third propellers and reduced lift for the third and fourth propellers, compared to the isolated propeller.
- Lift loss along the fuselage span due to propeller wake interference was confirmed. The simulations also indicated a limited lift increase on the wing at negative angles of attack, which requires further investigation.
- The downwash from the propellers on the horizontal stabilizer produces negative lift, creating a significant destabilizing pitching moment.
- There is preliminary evidence suggesting a limited effect of fuselage presence, which reduces the lift generated by the rear propellers.
- A methodology for calculating static stability derivatives for the full configuration was successfully developed. Using the obtained aerodynamic loads with the propellers, aerodynamic coefficients can be derived for the full aircraft.
- The methodology for calculating dynamic stability derivatives for the configuration without the propellers was investigated. The dependency of pitching oscillation frequency and amplitude on dynamic stability derivatives was investigated revealing a strong dependency on frequency. Since this was unexpected, the necessity to revise the methodology was identified.

Given the FSTD(H) requirement of a 5% tolerance on collective control position for low airspeed HQ, preliminary results demonstrated that completely neglecting aerodynamic interference between eVTOL components in the modeling will most probably result in thrust values outside this tolerance. All above-mentioned items will introduce modelling errors, which will be fully quantified in the future, through validation with experimental results, to decide whether they will be considered in the modeling or quantified as epistemic uncertainty in the model fidelity assessment.

Author contact: Agata Rylko agata.rylko@polimi.it, Marco Lovera marco.lovera@polimi.it, Giuseppe Quaranta giuseppe.quaranta@polimi.it

ACKNOWLEDGMENTS

The work in this study done by Agata Rylko was carried out within the 38th cycle of doctoral study in aerospace engineering, in research field ”Policy making for Urban Air Mobility acceptance” and received funding from PIANO NAZIONALE DI RIPRESA E RESILIENZA (PNRR). The work in this study done by Giuseppe Quaranta was carried out within the MOST -– Sustainable Mobility National Research Center and received funding from the European Union Next-Generation EU (PIANO NAZIONALE DI RIPRESA E RESILIENZA (PNRR) – MISSIONE 4 COMPONENTE 2, INVESTIMENTO 1.4 – D.D. 1033 17/06/2022, CN00000023). This manuscript reflects only the authors’ views and opinions, neither the European Union nor the European Commission can be considered responsible for them.

REFERENCES

1. Anon., *SC-VTOL, Special Condition for small-category VTOL aircraft, Issue 1*, EASA, 2019.
2. Anon., *Third Publication of Means of Compliance with Special Condition VTOL, MOC-3 SC-VTOL Issue 2*, Cologne, Germany, EASA, 2023.
3. Mitchell, D. G., Klyde, D. H., Shubert, M. W., Sizoo, D., and Schaller, R., “Testing for Certification of Urban Air Mobility Vehicles,” AIAA SciTech Forum, 2022.
4. Anon., *ADS-33E-PRF, Aeronautical Design Standard Performance Specification Handling Qualities Requirements for Military Rotorcraft*, United States Army Aviation and Missile Command Aviation Engineering Directorate, Redstone Arsenal, Alabama, 2000.

5. Anon., *ED-295, Guidance on VTOL Flight Control Handling Qualities Verification*, EUROCAE, 2024.

6. Lu, L., van't Hoff, S., Padfield, G., Podzus, P., Quaranta, G., and White, M., *Rotorcraft Certification by Simulation and Analysis; an Introduction to the Principles and Practices*, Springer, to be published, 2023.

7. Anon., *CS-FSTD(H), Certification Specifications for Helicopter Flight Simulation Training Devices*, EASA, 2012.

8. Mauery, T., Alonso, J., Cary, A., Lee, V., Malecki, R., Mavriplis, D., Medic, G., Schaefer, J., and Slotnick, J., "NASA/CR-20210015404, A Guide for Aircraft Certification by Analysis," Technical report, NASA, 2021.

9. Willis, J. B., "Trajectory Generation and Tracking Control for Winged Electric Vertical Takeoff and Landing Aircraft," Technical report, Theses and Dissertations, Brigham Young University, Utah, United States, 2021.

10. Tugnoli, M., Montagnani, D., Syal, M., Droandi, G., and Zanotti, A., "Mid-fidelity approach to aerodynamic simulations of unconventional VTOL aircraft configurations," *Aerospace Science and Technology*, Vol. 115, 2021. DOI: 10.1016/j.ast.2021.106804.

11. Masarati, P., Quaranta, G., Lanz, M., and Mantegazza, P., "Dynamic characterization and stability of a large size multibody tiltrotor model by pod analysis," International Design Engineering Technical Conferences and Computers and Information in Engineering Conference, Vol. 37033, 2003.

12. Quaranta, G., Masarati, P., and Mantegazza, P., "Multibody analysis of controlled aeroelastic systems on parallel computers," *Multibody System Dynamics*, Vol. 8, 2002, pp. 71–102.

13. Martinelli, E., *Modelling, control, integration and testing of an eVTOL drone*, Master's thesis, Politecnico di Milano, Italy, 2022.

14. Granata, D., Savino, A., and Zanotti, A., "Numerical Evaluation of Aircraft Aerodynamic Static and Dynamic Stability Derivatives by a Mid-Fidelity Approach," *Aerospace*, Vol. 11, (3), 2024. DOI: 10.3390/aerospace11030213.

15. Montagnani, D., Tugnoli, M., Fonte, F., Savino, A., Cocco, A., and Colli, A., *DUST User Manual*, 2023.

16. Piszkin S., T., and Levinsky E., S., "Nonlinear lifting line theory for predicting stalling instabilitites on wings of moderate aspect ratio," Technical report, General Dynamics Convair Division, San Diego, United States, 1976.

17. Bara, K., *Aerodynamics, propulsion and testing of an eVTOL drone*, Master's thesis, Politecnico di Milano, Italy, 2023.